

# Application of iron-oxide chemistry in mineral exploration

Georges Beaudoin

Département de géologie et de génie géologique, Université Laval, Québec, Québec G1V 0A6  
Author e-mail: Georges.Beaudoin@ggl.ulaval.ca

The iron oxides (magnetite and hematite) form major to accessory minerals in a range of mineral deposits and rocks. Iron oxides incorporate a large suite of minor to trace elements in their crystalline structure as a function of the thermodynamic conditions during crystallization. This variation in mineral composition is used to fingerprint a range of magmatic, hydrothermal and sedimentary mineral deposit types. Because iron oxides are resistant to mechanical abrasion and chemical alteration during transport and burial in sediments, and because they can be easily separated in magnetic fractions, they constitute a useful indicator mineral for exploration.

## ANALYTICAL METHODS AND SAMPLE PREPARATION

The mineral grains were analyzed using the highly optimized analytical methods of the Electron Probe Micro-Analyzer (EPMA; Dupuis & Beaudoin 2011) and Laser Ablation Inductively Coupled Plasma Mass Spectrometry (LA-ICP-MS; Dare *et al.* 2012). EPMA analyses have detection limits to 10s ppm for small areas (beam diameter of 10  $\mu\text{m}$ ), which is sufficient to avoid small inclusions in a target mineral. LA-ICP-MS analyses have detection limits to ppb levels, but the required volume is larger; during analyses a linear trench is typically ablated with a 80  $\mu\text{m}$ -diameter laser beam. This larger area required for analysis by LA-ICP-MS limits analyses to larger grains that are devoid of abundant inclusions. An advantage of the larger beam size of LA-ICP-MS is that small exsolutions formed by sub-solidus processes are incorporated in the mineral analysis, allowing measurement of the original composition of the grain before sub-solidus exsolution. Dare *et al.* (2012) indicated that both methods produce highly correlated analytical results down to the detection limit of the EPMA method.

For this study, bedrock samples were crushed to mimic the mechanical ablation produced by glaciers. The 0.5 to 2.0 mm heavy mineral ferromagnetic fractions of the till and disaggregated rock samples were prepared following the methods outlined by McClenaghan (2011). A representative subsample of grains from this ferromagnetic fraction was mounted in epoxy for EPMA analysis. These grains typically consisted of aggregates of one ferromagnetic mineral. Grains of less than 0.5 mm diameter do not have sufficient surface area for EPMA or LA-ICP-MS analyses and grains larger than 2.0 mm typically do not occur in sufficient numbers to be a representative subset. Statistical analysis indicates that in a subsample of  $\sim 100$  grains, approximately 70% of these grains will have a polished surface large enough for analysis, which is a sufficient number to determine a chemical composition representative of the sample as a whole (Sappin *et al.* 2012).

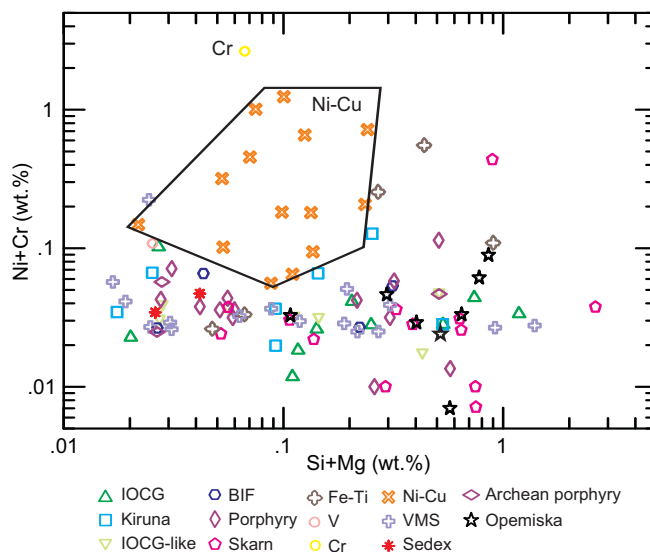
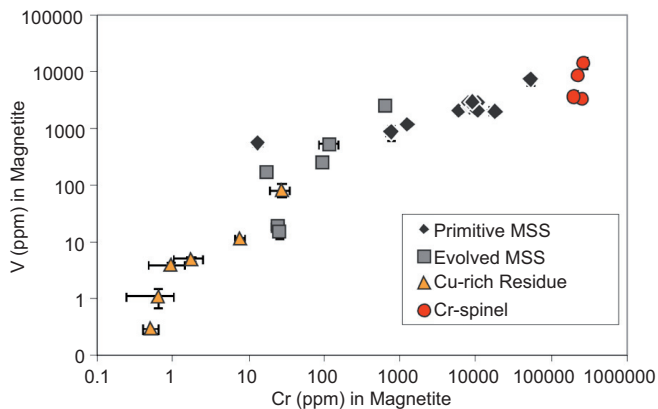


Fig. 1. The Ni+Cr versus Si+Mg discriminant diagram for Ni-Cu-PGE deposits (modified from Dupuis & Beaudoin 2011).

## IRON OXIDES IN MINERAL DEPOSITS

Dupuis & Beaudoin (2011) constructed a series of discriminant diagrams using the average composition a deposit type to identify the distinct composition of iron oxides in a variety of deposit types. Dupuis & Beaudoin (2011) showed that Ni-Cu-PGE deposits can be distinguished from all other deposit types using the Ni+Cr versus Si+Mg diagram (Fig. 1). Further work on Ni-Cu deposits incorporating deposits with large ranges of age, magma types, and geological environments, including most major Ni-Cu deposits worldwide, has confirmed the efficiency of the Ni+Cr versus Si+Mg discriminant diagram (Boutroy *et al.* 2012).

A study of Ni-Cu deposits from the Sudbury district showed that the composition of magnetite evolves during the fractional crystallization of the sulphide liquid into the early Fe-rich monosulphide solid solution (MSS) cumulate and the residual Cu-rich intermediate solid solution (ISS; Dare *et al.* 2012). Lithophile elements are compatible in magnetite. Magnetite co-crystallization with MSS depletes the residual ISS in lithophile elements such that later forming magnetite, co-crystallized with ISS, is also depleted in lithophile elements (Fig. 2). This pattern is found in Ni-Cu deposits worldwide (Boutroy *et al.* 2012). The efficiency of the Ni+Cr versus Si+Mg diagram is in part a consequence of the contrasting behaviour of lithophile Cr and chalcophile Ni. Spider diagrams of lithophile elements (Fig. 3A) and chalcophile elements (Fig. 3B) show that most lithophile elements, such as Cr, that are enriched in MSS magnetite become depleted in the residual sul-



**Fig 2.** Covariation of lithophile elements in magnetite in the sulphide liquid during fractional crystallization from MSS to ISS and chrome spinel (Cr-spinel) crystallized from the mafic magma in Sudbury (modified from Dare *et al.* 2012).

phide melt forming ISS magnetite (Fig. 3A; Dare *et al.* 2012). In contrast, chalcophile elements, such as Ni, partition preferentially in the MSS depleting the coeval magnetite; whereas, the late-forming magnetite in the ISS preferentially incorporates Ni in the absence of competing Fe-sulphides (Fig. 3B; Dare *et al.* 2012). Boutroy *et al.* (2012) also showed that secondary magnetite in veins in massive sulphide bodies and disseminated in host rocks has a composition that is different from that of primary magmatic magnetite and, as Figure 1 shows, plots outside the field typical for Ni-Cu-PGE deposits.

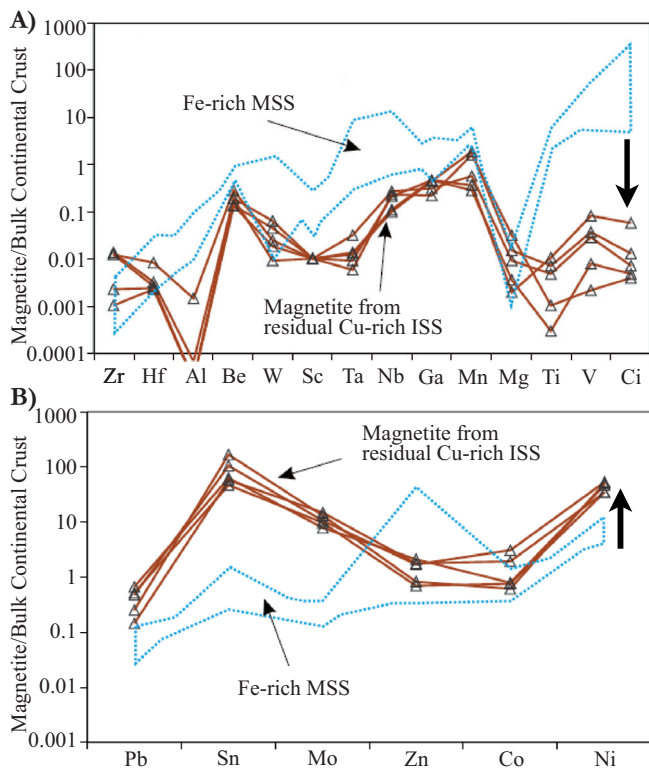


**Fig 3.** Spider diagrams of (A) lithophile and (B) chalcophile elements in MSS and ISS, normalized to bulk continental crust (Rudnick & Gao 2003). Arrows shows depletion of lithophile Cr (A), and enrichment of Ni (B), during fractional crystallization of the sulphide liquid from MSS to ISS (modified from Dare *et al.* 2012).

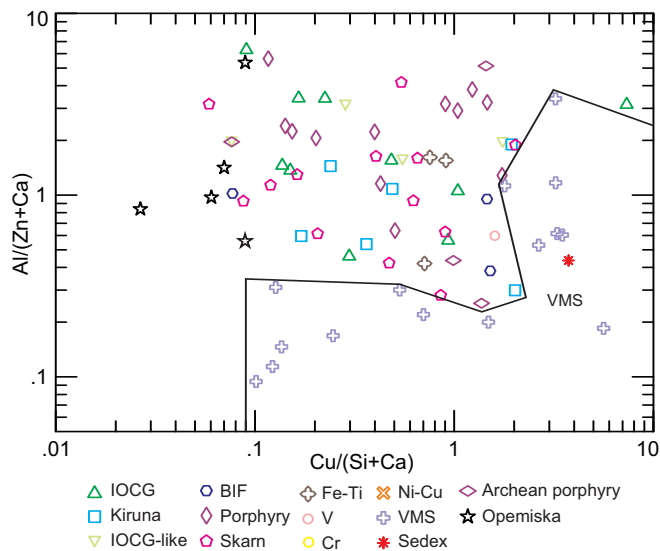


**Fig 4.** The Cu/(Si+Ca) versus Al/(Zn+Ca) discriminant diagram for Cu-Zn VMS and Zn-Pb SEDEX deposits (modified from Dupuis & Beaudoin 2011). Note that deposit average compositions that plot in the field for Ni-Cu deposits (Fig. 1) are not shown on this diagram.

The second step of data analysis is to test for iron oxides typical of Cu-Zn volcanogenic massive sulphide (VMS) and Zn-Pb SEDEX deposits using the Cu/(Si+Ca) versus Al/(Zn+Ca) diagram (Fig. 4; Dupuis & Beaudoin 2011). Magnetite in VMS and SEDEX deposits is typically a product of hydrothermal or metamorphic oxidation and replacement in the massive sulphide lens (Galley *et al.* 2000). In VMS deposits, magnetite is enriched in Si, Zn, and Ca, and depleted in Al, compared to other deposit types.

The final step of data analysis is to plot iron oxide compositions on the Ti+V versus Ni/(Cr+Mn) diagram (Fig. 5) to identify compositions typical of Fe-Ti-V, Kiruna Fe-P, Cu-Mo-Au porphyry, iron-oxide-copper-gold (IOCG), Superior-type banded iron formation and skarn deposit types (modified from Dupuis & Beaudoin 2011). Note that deposit average compositions that plot in the field for Ni-Cu deposits (Fig. 1) and in the field for VMS and SEDEX deposits (Fig. 4) are not shown on this diagram.

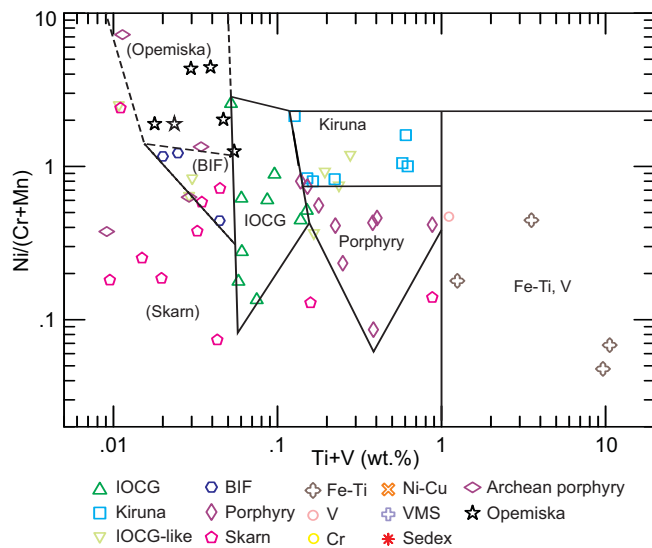


**Fig 5.** The Ti+V versus Ni/(Cr+Mn) discriminant diagram for Fe-Ti-V, Kiruna Fe-P, Cu-Mo-Au porphyry, iron-oxide-copper-gold (IOCG), Superior-type banded iron formation and skarn deposit types (modified from Dupuis & Beaudoin 2011). Note that deposit average compositions that plot in the field for Ni-Cu deposits (Fig. 1) and in the field for VMS and SEDEX deposits (Fig. 4) are not shown on this diagram.

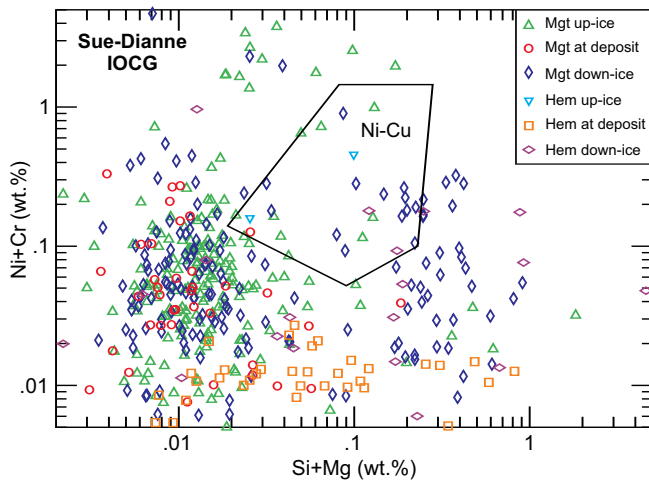


**Fig 6.** Magnetite and hematite composition from the ferromagnetic fraction of glacial tills up-ice, at the Sue-Dianne deposit (Great Bear Magmatic Zone, Northwest Territories, Canada) and down-ice, plotted in the Ni+Cr versus Si+Mg discriminant diagram for Ni-Cu-PGE deposits.

Au porphyry, iron-oxide-copper-gold (IOCG), Superior-type banded iron formation (BIF), and skarn deposit types (Dupuis & Beaudoin 2011). In this diagram, magmatic Fe-Ti-V deposits plot at high Ti+V values, whereas magmatic-hydrothermal and sedimentary deposits are characterized by lower Ti+V values (Fig. 5). Another diagram using Ti+V versus Ca+Al+Mn yields similar results (Dupuis & Beaudoin 2011).

#### APPLICATION TO MINERAL EXPLORATION

Two case studies serve to illustrate the application of iron-oxide chemistry of the ferromagnetic fraction of till samples. The Sue-Dianne deposit is a hematite-dominant IOCG deposit located in the Great Bear Magmatic Zone (Northwest Territories, Canada). In this region, the potential for Ni-Cu deposits is low and there are no showings known of this deposit type. Figure 6 illustrates that hematite and magnetite from till samples collected up- and down-ice of the Sue-Dianne IOCG deposit, plot with few exceptions outside the field for Ni-Cu deposits on a Ni+Cr versus Si+Mg discriminant diagram. A similar survey along a profile up- and down-ice of the Thompson Nickel Belt (Manitoba, Canada), near the Pipe Ni-Cu deposit open pit, is shown in Figure 7. In contrast to the rare occurrence of oxide grains with the signature of Ni-Cu deposits near the Sue-Dianne IOCG deposit, the survey across the Pipe open pit shows a high proportion of iron oxide grains with this signature (Fig. 7).

#### CONCLUSIONS

Iron oxides have a chemical composition that is reflective of the environment at the time of their formation. Fractional

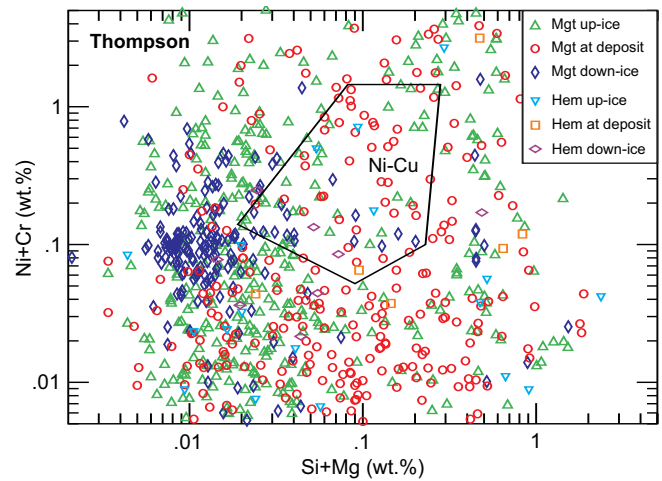


**Fig 7.** Magnetite and hematite composition from the ferromagnetic fraction of glacial tills up-ice, at the Pipe deposit (Thompson, Manitoba, Canada) deposit and down-ice, plotted in the Ni+Cr versus Si+Mg discriminant diagram for Ni-Cu-PGE deposits.

crystallization of magma and sulphide liquid can be tracked by the change in composition of the iron oxides, which affords new tools to access the fertility of an intrusion for Ni-Cu deposits. Different deposit types have distinct iron oxide chemical signatures that can be used to identify the trace of an eroded deposit in a surficial sedimentary environment (fluvial, eolian, or glacial).

#### REFERENCES

- BOUTROY, E., DARE, S.A.S., BEAUDOIN, G. & BARNES, S.-J. 2012. *Minor and trace element composition of magnetite from Ni-Cu deposits worldwide and its application to mineral exploration*. Geological Association of Canada-Mineralogical Association of Canada, Annual Meeting Program with Abstracts.
- DARE, S.A.S., BARNES, S.-J. & BEAUDOIN, G. 2012. Variation in trace element content of magnetite crystallized from a fractionating sulfide liquid, Sudbury, Canada: Implications for provenance discrimination. *Geochimica et Cosmochimica Acta*, **88**, 27–50.
- DUPUIS, C. & BEAUDOIN, G. 2011. Discriminant diagrams for iron oxide trace element fingerprinting of mineral deposit types. *Mineralium Deposita*, **46**, 319–335.
- GALLEY, A.G., JONASSON, I.R. & WATKINSON, D.H. 2000. Magnetite-rich calc-silicate alteration in relation to synvolcanic intrusion at the Ansil volcanogenic massive sulfide deposit, Rouyn-Noranda, Quebec, Canada. *Mineralium Deposita*, **35**, 619–637.
- MCCLLENAGHAN, M.B. 2011. Overview of common processing methods for recovery of indicator minerals from sediment and bedrock in mineral exploration. *Geochemistry: Exploration, Environment, Analysis*, **11**, 265–278.
- RUDNICK, R.L. & GAO, S. 2003. Composition of the continental crust. In: RUDNICK, R.L. (ed.) *The Crust*. In: HOLLAND, H.D. & TUREKIAN, K.K. (eds) *Treatise on Geochemistry*. Elsevier, **3**, 1–64.
- SAPPIN, A.-A., DUPUIS, C., BEAUDOIN, G. & McMARTIN, I. 2012. *Grain size fraction and number of grains representative of iron oxide composition in till samples: the Sue-Dianne deposit area, Northwest Territories, Canada*. Geological Association of Canada-Mineralogical Association of Canada-Society of Economic Geology-Annual Meeting, Program with Abstracts.

